JOURNAL OF GUIDANCE, CONTROL, AND DYNAMICS
Vol. 15, No. 4, July-August 1992

Thrust Laws for Microburst Wind Shear Penetration

Mark L. Psiaki* and Kihong Park†
Cornell University, Ithaca, New York 14853

Two thrust guidance strategies have been developed and analyzed for the ability that they give aircraft to safely penetrate microburst wind shear during landing approach. These are used in conjunction with a pitch steering strategy that has already been shown to give improved performance by maintaining nominal glide slope in the presence of microburst winds. The strategies provide valuable understanding of good thrust policy in a microburst. One of the two strategies is to control the airspeed to its nominal value, and the other strategy is to control the airspeed or the inertial speed, whichever is smaller, to the nominal value. Two longitudinal aircraft models have been used to evaluate these strategies, a simplified first-order model and a sixth-order model. Several idealized microburst models have been used to simulate representative encounters. Also, glide-slope tracking performance over a range of microbursts has been plotted and compared with that of optimal trajectories. The thrust laws' performance is not as good as that of optimal trajectories, as expected; the thrust guidance laws do not use the global knowledge of the wind field that the optimal trajectories use. Nevertheless, the ability of the more practical strategies to safely penetrate severe microburst wind shear has been demonstrated. The best performing guidance law is the one that controls the minimum of airspeed and inertial speed to a nominal value. This demonstrates the importance of using thrust to keep the inertial speed at or above the nominal value.

Introduction

THE objective of this work is to develop and evaluate guidance strategies that minimize the danger of inadvertent microburst encounter on landing approach. The hazard that microbursts pose to aviation is well documented.[1,2] The safest strategy for dealing with microbursts is probably to detect and avoid them, but safety could be further improved through improvement of piloting strategies for dealing with inadvertent encounters[3,4]; such encounters will continue to occur even with increased detection/warning capabilities.

The guidance laws developed in this paper are concerned with flight in the vertical plane; they dictate the thrust and pitch commands. The effects of microbursts on symmetric flight have generally been found to pose the greatest threat. A good pitch steering strategy has already emerged from previous work.[4,5] This paper concentrates on the development and evaluation of two thrust strategies for use in conjunction with that pitch steering strategy. These strategies have been developed based on extensive experience with optimal microburst encounter trajectories.[5]

Recent efforts to improve control strategies for wind shear encounter include those of Miele et al.,[6-10] Zhao and Bryson,[11,12] Psiaki,[5] and Psiaki and Stengel.[4,13,14] All of these groups have considered either landing approach or takeoff, or both, the two flight phases where wind shear can prove dangerous. All of these groups have used trajectory optimization to determine the best possible piloting strategy in microburst situations, given global knowledge of the wind shear. These studies differ somewhat in the objectives of the optimization. Miele et al.[9] include the flare maneuver in the landing-approach cost function. Zhao and Bryson[11] have distinguished between two cases: performance encounter (low-to-moderate intensity microbursts) and survival encounter (high-intensity microbursts). Psiaki[5] and Psiaki and Stengel[4] have spent considerable effort on developing and using a methodology for determining the range of wind shear cases through which safe flight is possible for a given optimally controlled aircraft. They call this type of study a performance evaluation of microburst encounter capabilities. Miele et al.[6,8-10] have also done considerable work on development and evaluation of practical guidance laws; currently practical strategies can rely only on local knowledge of the wind shear. Zhao and Bryson[12] have worked on practical strategies for the takeoff case.

The present work is an extension of the work of Psiaki and of Psiaki and Stengel into the realm of practical guidance. Two alternative landing-approach thrust strategies are developed to augment a pitch steering strategy that has already been developed. They are somewhat different than the guidance strategy proposed by Miele et al.[9] The proposed strategies are studied by simulating representative microburst encounters and by determining the range of microbursts through which they can fly safely. This latter study is a simplified version of Psiaki and Stengel's performance evaluation technique.

The remainder of this paper is divided into four sections plus conclusions. The second section gives the aircraft and microburst models used in the study. This includes a simplified first-order model of the speed response to thrust inputs, which gets used in the subsequent performance study. The third section reviews the simplified performance calculations described in Refs. 4 and 5. The fourth section presents the two proposed thrust guidance strategies and reviews the pitch strategy that has been adapted from Refs. 4, 5, and 14. The fifth section concludes the body of the work by presenting the performance results for each strategy along with examples of trajectories generated by the proposed strategies.

Microburst Encounter Modeling

Aircraft Dynamic Model

The longitudinal translational motions of an aircraft in a wind shear can be modeled by a system of four coupled nonlinear ordinary differential equations:

$$\dot{V}_i = \left\{\frac{1}{m}\right\}\{-\bar{q}S[C_D\cos(\alpha_i - \alpha_a) + C_L\sin(\alpha_i - \alpha_a) + T\cos(\alpha_i + i_T)\} - g\sin\gamma_i$$

Presented as Paper 89-3560 at the AIAA Guidance, Navigation, and Control Conference, Boston, MA, Aug. 14-16, 1989; received July 11, 1990; revision received July 1, 1991; accepted for publication July 10, 1991.

*Assistant Professor, Department of Mechanical and Aerospace Engineering. Member AIAA.

†Graduate Student, Department of Mechanical and Aerospace Engineering.

$$\dot{\gamma}_i = \left\{\frac{1}{V_i}\right\}\left(\left[\frac{1}{m}\right]\{\bar{q}S[C_L\cos(\alpha_i-\alpha_a) - C_D\sin(\alpha_i-\alpha_a)] + T\sin(\alpha_i+i_T)\} - g\cos\gamma_i\right)$$

$$\dot{h} = V_i\sin\gamma_i$$

$$\dot{r} = V_i\cos\gamma_i \tag{1}$$

where V_i is inertial speed, γ_i is inertial flight-path angle, h is altitude, r is range, C_D is the drag coefficient, C_L is the lift coefficient, g is the acceleration of gravity, i_T is the angle between the thrust vector and the body-fixed x axis, m is the aircraft mass, S is the wing area, and T is the thrust. The effects of wind shear enter through the difference between the inertial and air-relative angles of attack, $\alpha_i - \alpha_a$, and through the airspeed and dynamic pressure, V_a and $\bar{q} = \rho V_a^2/2$:

$$\alpha_i - \alpha_a = \tan^{-1}\left(\frac{V_i\sin\gamma_i + w_v}{V_i\cos\gamma_i + w_h}\right) - \gamma_i$$

$$V_a = \sqrt{V_i^2 + w_v^2 + w_h^2 + 2V_i(w_v\sin\gamma_i + w_h\cos\gamma_i)} \tag{2}$$

where w_v is vertical wind speed (positive is a downdraft), and w_h is horizontal wind speed (positive is a headwind). The quantity ρ is the air density. The lift and drag models are

$$C_L = C_{L_0} + C_{L_\alpha}\alpha_a$$

$$C_D = C_{D_0} + \epsilon C_L^2 \tag{3}$$

where the aerodynamic coefficients C_{L_0}, C_{L_α}, C_{D_0}, and ϵ are modeled as constants. The air-relative angle of attack and the thrust setting act as control inputs to this fourth-order model.

First-Order Dynamic Model

A significant simplification of the aircraft dynamic model can be implemented given the pitch control law suggested by previous work[4,5,14] coupled with a change of independent variable from time to range. The pitch control law is intended to minimize the deviation from the intended touchdown point by keeping to the nominal glide slope. Taken to its extreme, this strategy yields an α_a (hence C_L) input that gives $\dot{\gamma}_i = 0$. Thus, the nominal flight-path angle γ_{i_0} can be substituted into the first, third, and fourth of Eqs. (1), and the second of these equations need not be integrated. The fourth equation can be eliminated by changing to range as the independent variable. The first and third equations are divided by the fourth equation; V_i is assumed never to vanish, and the wind field is assumed to be time invariant. Integration of the resulting dh/dr equation is trivial: $h = h_0 + (r - r_0)\tan\gamma_{i_0}$. This leaves a first-order dynamic model of the inertial velocity variation with the range

$$\frac{dV_i}{dr} = \left(\frac{1}{V_i\cos\gamma_{i_0}}\right)\left(\left\{\frac{1}{m}\right\}\{-\bar{q}S[C_D\cos(\alpha_i-\alpha_a) + C_L\sin(\alpha_i-\alpha_a)] + T\cos(\alpha_i+i_T)\} - g\sin\gamma_{i_0}\right)$$

$$\equiv f_i(V_i, r, T) \tag{4}$$

where V_i is the dependent variable, r is the independent variable, and T is the control input.

All quantities in Eq. (4) depend on just V_i, r, and T. The quantities V_a, $\bar{q}$, and $\alpha_i - \alpha_a$ depend only on V_i and the wind terms, w_v and w_h [Eqs. (2)], but the wind terms depend only on r and h, and h depends on r. Therefore, airspeed, dynamic pressure, and the difference between inertial and air-relative angle of attack depend only on r and V_i. The quantities C_L, C_D, and α_i are functions of V_i, r, and T because of the pitch "control law," $\dot{\gamma}_i = 0$, the aerodynamic model, Eqs. (3), and the relationship between air-relative and inertial angle of attack, Eq. (2).

This model is closely related to two models from classical aircraft dynamics. One is the static model used to analyze the power required to fly at a given airspeed.[15] The other is the dynamic model which shows that, on the back side of the power curve without power feedback, altitude control with the pitch input destabilizes airspeed.[16]

Sixth-Order Dynamic Model

Whereas a simplified model is needed to allow efficient study of a variety of microburst encounters, a more complex model is needed to add a degree of realism that brings credibility to the study. A sixth-order model has also been used in this study. It adds simplified first-order models of the engine dynamics and the closed-loop pitching motions. Figure 1 presents block diagrams for these two models. Each is a first-order lag, with rate limiting, between the commanded value of thrust or angle of attack and the actual value:

$$\dot{T} = \begin{cases} 10(T_c - T) & \text{if } -0.3 \le 10(T_c - T) \le 0.3 \\ 0.3 & \text{if } 0.3 < 10(T_c - T) \\ -0.3 & \text{if } 10(T_c - T) < -0.3 \end{cases} \tag{5}$$

$$\dot{\alpha}_a = \begin{cases} 10(\alpha_{a_c} - \alpha_a) & \text{if } -0.052 \le 10(\alpha_{a_c} - \alpha_a) \le 0.052 \\ 0.052 & \text{if } 0.052 < 10(\alpha_{a_c} - \alpha_a) \\ -0.052 & \text{if } 10(\alpha_{a_c} - \alpha_a) < -0.052 \end{cases} \tag{6}$$

where the subscript c refers to commanded values as opposed to actual values. The time constants of the loops may seem fast (0.1 s), but the rate limits are reasonable—30% of maximum thrust/s ($|\dot{T}| \le 0.3 \cdot T_{max}$/s) and 3 deg/s ($|\dot{\alpha}_a| \le 0.052$ rad/s).

Microburst Wind Shear Models

A microburst is a vertical column of descending air that spreads out in a horizontal outflow as it hits the ground.[17] The vertical jet is thermally induced. The two main hazards to aviation are the downdraft and the horizontal outflow. The downdraft forces an aircraft towards the ground, and the outflow causes an aircraft to experience a shear from a headwind to a tailwind, no matter which way it traverses the wind field. The length scale, the intensity, and the relative importance of the downdraft vs the headwind/tailwind shear all can vary between different microburst encounters.

For purposes of performance analysis, the engineering approximation microburst models of Psiaki and Stengel[4] and Psiaki[5] are used. One is a headwind/tailwind shear. The wind speed depends only on range and varies from a headwind to a tailwind as one period of a sine wave, Fig. 2 (left-hand axis).

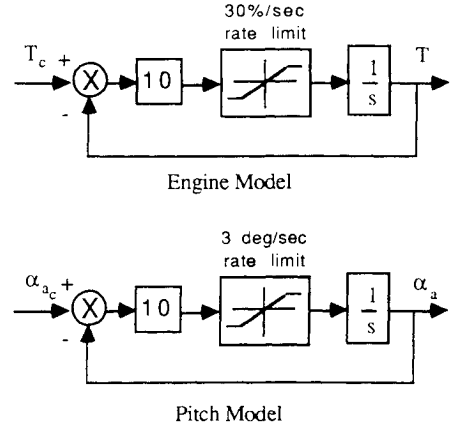

Fig. 1 Block diagrams of engine and pitch dynamic models.

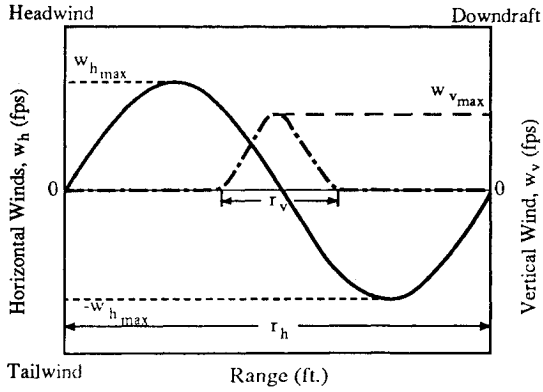

Fig. 2 Dependence of wind speed on range for two simplified microburst wind models: headwind/tailwind and downdraft.

The other model is a downdraft shear. The downdraft depends only on range and varies as one period of a 1-cosine wave (a pulse), Fig. 2 (right-hand axis). The quantities r_h and r_v specify the length scales of these two microburst types. The parameters $w_{h_{max}}$ and $w_{v_{max}}$ specify their intensities. These two models idealize the two threats posed by a microburst. Yet, they can be characterized by a small number of parameters, which greatly simplifies performance analysis. A combination of these models has been found to capture the basic effects of an actual microburst on an aircraft trajectory.[14] These models are somewhat different from the model used by Miele et al. (see Ref. 9, for example) and from the model used by Zhao and Bryson.[11] For comparison purposes, simulation results for encounter with Miele-type microbursts are also presented.

Performance Analysis (Simplified)

Psiaki and Stengel[4] and Psiaki[5] have developed a method of microburst encounter performance analysis. For a given aircraft/guidance law, the method distinguishes microbursts that can be safely transited from those that cannot be safely transited. Performance can be characterized conservatively by contours of various safety-related quantities plotted in a two-dimensional microburst length-scale, intensity space. Each point in this parameter space corresponds to a particular aircraft trajectory through a particular microburst. The trajectory's worst-case values of various safety-indicating quantities (e.g., maximum deviation from the intended glide slope, maximum inertial velocity) characterize the hazard at that point in microburst parameter space.

This paper is concerned primarily with the maximum altitude deviation performance and uses a simplified method of calculating it. Short landing has been a typical mode for accidents caused by microburst encounter on landing approach.[1,2] One way to avoid a short landing is to closely track the intended glide slope.

A simplified way has been found to determine a contour that separates microbursts into two categories: safer microbursts, which allow good glide-slope tracking, and more dangerous microbursts, which cause significant excursions below the intended glide slope.[5] The way to generate this contour is to do simulations of encounters with various microbursts, modeling the aircraft/pitch law via Eq. (4) while simulating the thrust control strategy. The maximum C_L that occurs during each simulation is a function of the microburst parameters for that simulation. One contour of this function corresponds to the value $C_{L_{max}}$ (maximum of the lift curve), and it is the contour that distinguishes between safer and more dangerous glide-slope tracking performance.[5] When C_L exceeds the stall limit during simulations of Eq. (4), the results become meaningless, but the trajectories up to and including the contour of interest remain valid. This analysis can be extended to account for flare capability by setting the performance contour at a lower C_L value, one that reserves a lift-coefficient margin for the flare maneuver.

Aircraft Guidance Laws in a Microburst Wind Shear

The problem of vertical-plane guidance in a microburst wind shear is caused by two microburst features, the outflow and the downdraft. In the zone between maximum headwind and maximum tailwind, the outflow robs the aircraft of airspeed. The downdraft adds to the aircraft descent rate. Both of these effects contribute to short landings. Neglecting the case of a decision to abort the landing, the first aim of any guidance law should be to apply pitch control and thrust control to cause touchdown to occur at the desired location. Once this has been guaranteed, other concerns can be handled, such as preserving lift margin for flare and limiting inertial velocity at touchdown.

The objective of the optimization work of Psiaki and Stengel[5] was to fly as close as possible to the nominal glide slope for the entire encounter. If possible, this would ensure touchdown at the desired point. Close glide-slope tracking turned out to be possible for some very intense wind shears. The aircraft used pitch control to maintain glide slope, varying angle of attack out of phase with airspeed to maintain lift approximately constant.

These results clearly indicate a desirable practical pitch control strategy: a high-gain feedback controller to maintain glide slope through pitch commands. The thrust control of the optimal microburst encounters, however, is less practical. It relies on global information about the wind field. In the most severe microbursts, the trajectory optimization algorithm calls for full thrust at the beginning of the microburst encounter because it knows about the strong tailwinds that will follow the headwinds, but no pilot would do this with only local information about the winds. A look-ahead wind shear detection system would be needed to implement the optimal strategy. Such systems are under development and may make the optimal strategy feasible someday.

The thrust strategy's purpose is to augment the pitch strategy by trying to keep the aircraft from running out of airspeed while pitch control is in the process of maintaining glide slope. (This emphasis on minimum airspeed does not imply that airspeed control is the overriding concern in a microburst. It is only an auxiliary concern that makes for an increased ability to maintain glide slope with pitch steering inputs.) One obvious strategy is to try a simple feedback in which thrust controls airspeed at the nominal. This is one of the two strategies that have been analyzed for this paper. This thrust strategy, in combination with the earlier pitch strategy, is similar in spirit to one developed by Lambregts for nonmicroburst wind shears.[18] In very intense microbursts, however, the thrust control will saturate, and the airspeed control strategy might not perform as well as others. For one thing, it does the opposite of what the optimal trajectories do in the headwind buildup section of a microburst: it lowers thrust to maintain airspeed whereas the optimal strategies raise thrust to prepare for the imminent tailwinds.

Another, almost as practical, thrust strategy takes inertial speed into account as well as airspeed, implicitly accounting for the wind speed. This strategy involves setting the same nominal value for airspeed and inertial speed. The thrust feedback loop is designed to keep the minimum of the two speeds at this nominal value. In a no-winds situation, the two speeds would be the same, and this controller would behave like an airspeed controller. In a microburst situation, the initial headwind buildup section would not cause the thrust to decrease because the minimum of the two speeds would be inertial speed and would be at the nominal. When the headwind shifted to a tailwind, the minimum speed would become airspeed, and to keep airspeed at the nominal, thrust would increase as long as tailwind was increasing.

The advantage of airspeed/inertial speed control over simple airspeed control is that it would not allow the aircraft's

inertial speed to bleed off in the headwind buildup section of a microburst. The aircraft would have no inertial velocity deficit when it entered the tailwind zone and would have more chance of keeping airspeed above the 1-g stall limit while maintaining glide slope with pitch control. Yet this scheme is equally practical, requiring only airspeed and inertial speed feedback signals and behaving normally in a no-winds situation. Some pilots may already be trained to use this strategy,[19] but other wind shear researchers, by their choice of initial conditions in trajectory optimizations and simulations, seem to indicate that this strategy may not be obvious.[9,11] Lambregts, in his energy management scheme, also ignores inertial speed in favor of airspeed during wind shear encounter: the strategy uses only rate of change of airspeed to compute the rate of change of total energy.[18]

The previous two thrust control strategies have been evaluated using both the first-order and the sixth-order aircraft models. The first-order model is used in conjunction with the performance evaluation scheme of the preceding section. To do this evaluation, the first-order model must be augmented with simplified thrust-control simulations. An expression for the derivative of the airspeed with respect to range is needed for development of these simplified laws. This is derived by squaring the second of Eqs. (2) and differentiating the result with respect to r, which yields a formula of the form $dV_a/dr \equiv f_a(V_i, r, T)$. An idealized model of the airspeed control law is to choose $T = T_a$, which is implicitly defined as the solution of

$$V_0 = V_a + \frac{1}{K}\left(\frac{dV_a}{dr}\right) = V_a(V_i, r) + \frac{1}{K}[f_a(V_i, r, T_a)] \tag{7}$$

for a given V_i and r. Minimum and maximum limits are also placed on T (0 and 100% of maximum, respectively, for the first-order model). The quantity K acts like a feedback gain so that T_a tries to null any airspeed error, $V_0 - V_a$, in $1/K$ feet of range. In addition to T_a, the airspeed/inertial speed control law computes the thrust to null out inertial speed errors, T_i, implicitly defined by

$$V_0 = V_i + \frac{1}{K}\left(\frac{dV_i}{dr}\right) = V_i + \frac{1}{K}[f_i(V_i, r, T_i)] \tag{8}$$

It chooses $T = \max(T_a, T_i)$, again subject to minimum and maximum limits on T. This latter control law achieves the intended goal, regulation to achieve $\min(V_a, V_i) = V_0$.

Simulation and performance results for the previous guidance strategies, in combination with the dynamic model in Eq. (4), are presented in the next section. One small exception is that $\alpha_i + i_T$, the angle between the thrust vector and the inertial velocity vector, has been assumed to be zero in the case of pure headwind/tailwind microbursts, which simplifies computation. In strong downdrafts, this assumption may be very inaccurate; hence, it has not been used for the downdraft microburst simulations.

Different models of the two proposed guidance laws are needed for use with the sixth-order aircraft model. Figure 3 gives the block diagrams for the overall system (top plot) and for the pitch and thrust loops (middle and bottom plots). The pitch control law can be modeled by the following equations:

$$\Delta h = \begin{cases} h_{\text{nom}}(r) - h & \text{if} \quad -50 \le h_{\text{nom}}(r) - h \le 50 \\ 50 & \text{if} \quad 50 < h_{\text{nom}}(r) - h \\ -50 & \text{if} \quad h_{\text{nom}}(r) - h < -50 \end{cases} \tag{9a}$$

$$\Delta\gamma = \gamma_{\text{nom}} - \gamma_i \tag{9b}$$

$$\alpha_{\text{rec}} = \begin{cases} (4.11\Delta\gamma + 0.00875\Delta h & \text{if} \quad -\alpha_{g_{\text{lim}}} \le (4.11\Delta\gamma + 0.00875\Delta h) \le \alpha_{g_{\text{lim}}} \\ \alpha_{g_{\text{lim}}} & \text{if} \quad \alpha_{g_{\text{lim}}} < (4.11\Delta\gamma + 0.00875\Delta h) \\ -\alpha_{g_{\text{lim}}} & \text{if} \quad (4.11\Delta\gamma + 0.00875\Delta h) < -\alpha_{g_{\text{lim}}} \end{cases} \tag{9c}$$

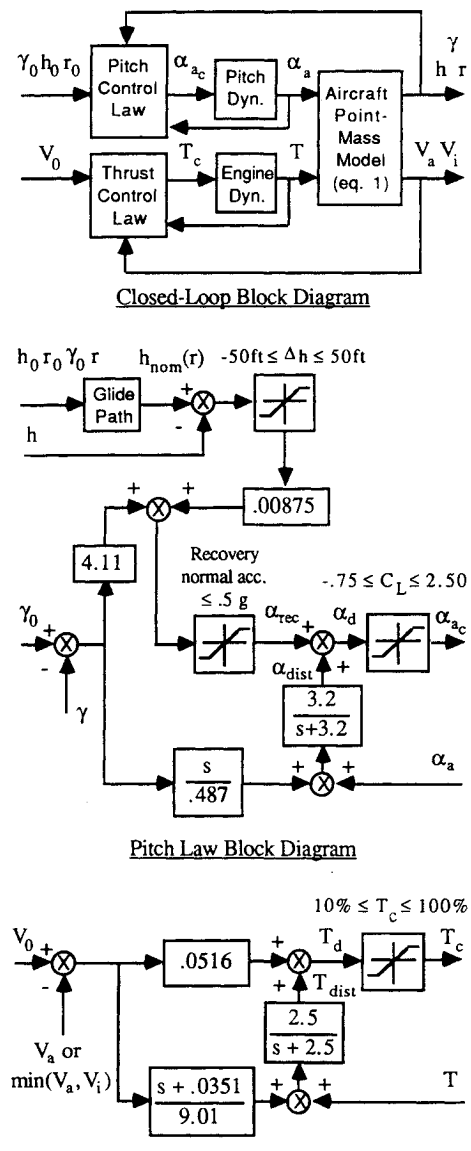

Fig. 3 Block diagrams for closed-loop control of the sixth-order aircraft model.

$$\alpha_{g_{\text{lim}}} = \frac{g}{2 \cdot 0.487 \cdot V_i} \tag{9d}$$

$$\dot{x}_7 = -3.2x_7 - 3.2\Delta\gamma + 0.487\alpha_a \tag{9e}$$

$$\alpha_{\text{dist}} = \frac{3.2}{0.487}(x_7 + \Delta\gamma) \tag{9f}$$

$$\alpha_{a_c} = \begin{cases} \alpha_{\text{rec}} + \alpha_{\text{dist}} & \text{if} \quad -0.419 \le \alpha_{\text{rec}} + \alpha_{\text{dist}} \le 0.226 \\ 0.226 & \text{if} \quad 0.226 < \alpha_{\text{rec}} + \alpha_{\text{dist}} \\ -0.419 & \text{if} \quad \alpha_{\text{rec}} + \alpha_{\text{dist}} < -0.419 \end{cases} \tag{9g}$$

The pitch law is basically a proportional-integral (PI) controller for both altitude and flight-path angle, which works out to a proportional-integral derivative (PID) law for altitude because γ_i is like $\dot{h}$. The upper saturation block on Fig. 3 limits the magnitude of the altitude error signal Δh [Eq. (9a)]. The

middle saturation block [Eq. (9c)] effectively limits the normal acceleration used during recovery from altitude deviations; α_{rec} is the portion of the desired angle of attack that causes acceleration in the direction of recovery. These two saturation blocks keep the controller stable for large errors by keeping it from trying to recover too rapidly from large altitude deviations. The lower part of the pitch law on Fig. 3 [Eqs. (9e) and (9f)] constitutes a reduced-order observer for flight-path disturbances; α_{dist} is the component of angle of attack that counteracts the estimated disturbance. This part of the control law effectively adds integral action; to see this, recall that α_a follows α_{a_c} and consider the effects of the positive feedback of α_a. In the lower right-hand corner of Fig. 3's pitch law there is another saturation block [Eq. (9g)]. It limits commanded angle of attack α_{a_c} to avoid stall. Antiwindup logic for the integral portion of the control law is effectively implemented by the feedback of angle of attack to the disturbance observer after it has passed through this saturation block.

The two thrust laws are also PI controllers with disturbance estimation, control saturation, and antiwindup logic similar to that of the pitch law. Depending on which thrust law is being used, either V_a or $\min(V_a, V_i)$ is the quantity that gets fed back to the thrust. The two thrust laws are modeled by the following equations:

$$\Delta V = V_0 - [V_a \text{ or } \min(V_a, V_i)] \tag{10a}$$

$$\dot{x}_8 = -2.5x_8 - 2.5\Delta V + 9.14T \tag{10b}$$

$$T_{dist} = 0.274x_8 + 0.277\Delta V \tag{10c}$$

$$T_c = \begin{cases} (0.0516\Delta V + T_{dist}) & \text{if } 0.1 \le (0.0516\Delta V + T_{dist}) \le 1.0 \\ 1.0 & \text{if } 1.0 < (0.0516\Delta V + T_{dist}) \\ 0.1 & \text{if } (0.0516\Delta V + T_{dist}) < 0.1 \end{cases} \tag{10d}$$

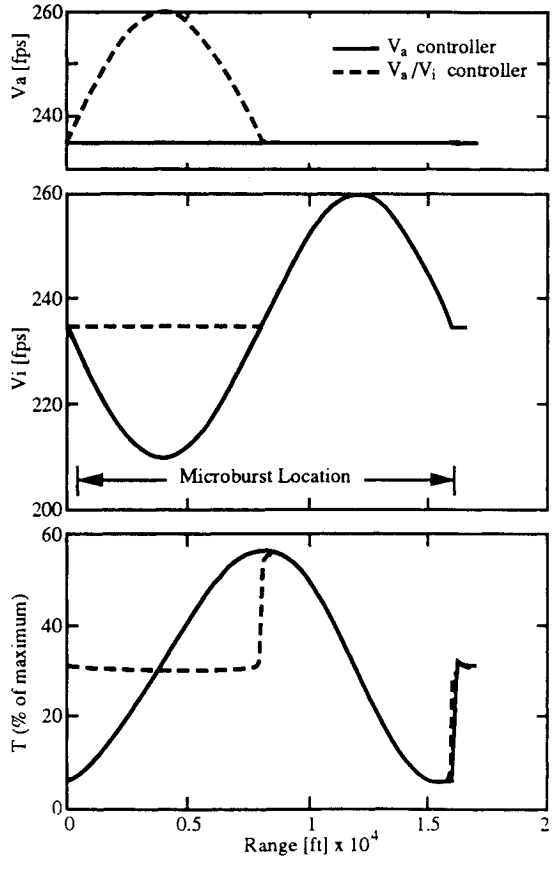

Fig. 4 First-order aircraft model and two thrust control laws in a headwind/tailwind microburst (r_h = 16,000 ft, $w_{h_{max}}$ = 25 fps).

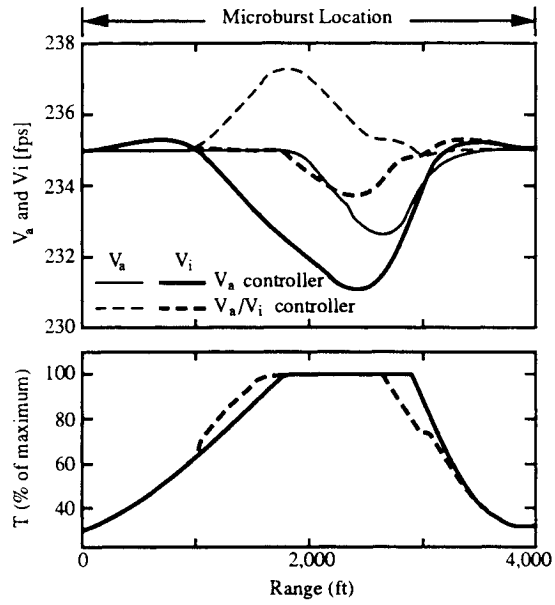

Fig. 5 First-order aircraft model and two thrust control laws in a downdraft microburst (r_v = 4000 ft, $w_{v_{max}}$ = 50 fps).

The closed-loop system is eighth order, and its linearization has eigenvalues (-9.54, -7.38, -3.96, $-1.77 \pm 0.50j$, -0.78, -0.54, and 0). The zero eigenvalue corresponds to the range mode. The aircraft is free to deviate in range as long as it follows the intended glide slope. The two fastest eigenvalues arise from the engine and pitch dynamic models.

The thrust law of Miele et al.[9] acts much like the airspeed-maintaining thrust law proposed in this paper, especially when one considers that their work does not consider the headwind buildup section of a microburst. They start their simulations with the aircraft in the peak headwind flying at the nominal airspeed. Thus, they are modeling the headwind buildup phase of the microburst encounter as having been transited under the supervision of a perfect airspeed controller. In the phase of shear from headwind to tailwind, full power is used to counteract the tremendous airspeed loss, just as with the airspeed controller.

Microburst Penetration Results for Two Thrust Guidance Laws

Simulation and performance analysis of the thrust guidance laws described earlier have been performed for a jet transport aircraft in the 150,000 lb class. The aircraft's properties are

m = 4,660 slugs
T_{max} = 42,000 lb
S = 1560 ft^2
i_T = 0 deg
C_{L_0} = 1.36
$C_{L_{max}}$ = 2.5
ϵ = 0.067
C_{L_α} = 5.04
C_{D_0} = 0.064

and the nominal landing-approach trajectory has $\gamma_{i_0} = -3$ deg and V_0 = 235 fps.

First-Order-System Microburst Encounter Examples

This section considers the results for some typical trajectories of the first-order model. Figure 4 presents some time histories for two encounters with the same microburst. The microburst is a headwind/tailwind microburst [Fig. 2 gives $w_h(r)$ function], and the two trajectories correspond to the two different thrust guidance laws: solid for the airspeed law (V_a law) and dashed for the airspeed/inertial-speed law(V_a/V_i law). From the top, the plots are airspeed, inertial speed, and

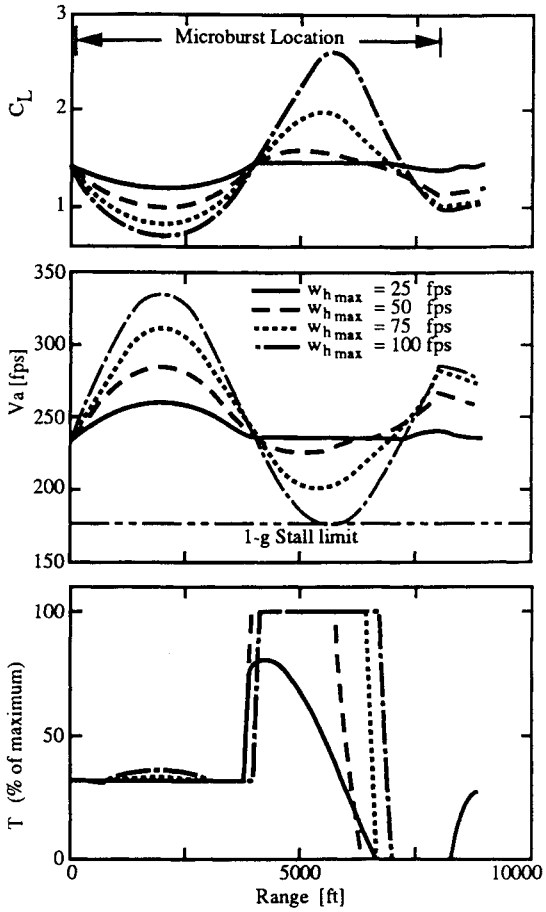

Fig. 6 Variation of V_a/V_i controller performance with headwind/tailwind microburst intensity (r_h = 8000 ft).

thrust, all plotted vs range. Plots of altitude vs range have been omitted because they always exactly follow the nominal glide slope when Eq. (4) is valid.

As can be seen, the thrust does not saturate for either controller, and each is able to achieve its intended purpose perfectly: the solid curve on the airspeed plot is flat at the nominal speed; the dashed curve on both the airspeed and inertial speed plots is either above the nominal speed or flat at the nominal speed. Whenever the dashed curve is above the nominal on the airspeed plot, it is at the nominal on the inertial speed plot and vice versa. Notice how the two curves coincide during the latter, tailwind half of the microburst. In this section, $V_a < V_i$ and the two control laws are identical. The two trajectories enter the tailwind zone with the same initial condition, which would not be the case if the microburst intensity were sufficient to cause the V_a controller to saturate thrust at 100% during the first half of the microburst.

Figure 5 presents time histories corresponding to the two guidance laws for encounter of another microburst. This microburst is a downdraft microburst [Fig. 2 gives $w_v(r)$ function]. Thrust saturation occurs in both cases, so neither controller is quite able to achieve its intended goal: note the excursions of various curves below 235 fps on the top plot of the figure. All speed curves except the solid, heavy line-weight curve (V_i for the V_a-guided case) should stay above 235 fps. The feedback gain K is relatively high, 1/(200 ft), which causes speed recovery to occur soon after saturation ceases. Notice that the V_a/V_i controller's encounter airspeed (and inertial speed) is always greater than or equal to that which occurs during V_a-guided encounter.

Time histories associated with penetration of four different microbursts are presented in Fig. 6. The four histories correspond to four different peak wind intensities and just one guidance scheme, V_a/V_i guidance. All of the microbursts are of the headwind/tailwind variety, and each has a length scale of 8000 ft. These results give a flavor of the calculations used to find simplified performance contours as described in the third section.

As the microburst peak headwind (and tailwind) intensity increases from 25 to 100 fps, the thrust activity (bottom plot) increases until saturation occurs in the tailwind zone. Along with this saturation goes a failure to meet the control goal: airspeed drops below the nominal in the tailwind zone (middle plot). Correspondingly, the lift coefficient rises above the nominal in this zone. The peak lift coefficient for each trajectory occurs in the tailwind zone, and this peak increases with peak microburst wind intensity, reaching 2.6 in the microburst that has 100 fps tailwinds (top plot). This peak is above the $C_{L_{max}}$ of the aircraft, so the trajectory corresponding to the 100 fps microburst is not meaningful; the pitch law assumption used in deriving Eq. (4) is not valid for $C_L > 2.5$. Thus, the simplified performance analysis indicates that the V_a/V_i-guided aircraft operating in r_h = 8000 ft headwind/tailwind microbursts is limited to a $w_{h_{max}}$ somewhat less than 100 fps.

Simplified Performance Results for Two Guidance Laws

Glide-slope tracking performance has been estimated by the simplified method, which uses the first-order aircraft model. Figure 7 presents performance contours for penetration of headwind/tailwind-type microbursts (top plot) and for penetration of downdraft-type microbursts (bottom plot). On each plot are three simplified performance contours, those for optimized trajectories taken from Refs. 4 and 5 (solid curves), those for V_a/V_i thrust guidance (dashed curves), and those for V_a thrust guidance (dotted curves). The V_a guidance curve in the top plot is discontinued above the headwind/tailwind microburst intensity of 235 fps because this equals the nominal airspeed and leads to nonsensical results in the headwind section.

Several similarities exist between the two plots. On both plots the performance contours associated with the two guidance laws lie well below the contours for the optimized trajectories. This is because the trajectory optimizer has global wind field information; therefore, it uses peak thrust earlier in each encounter. The two guidance laws do not call for full thrust

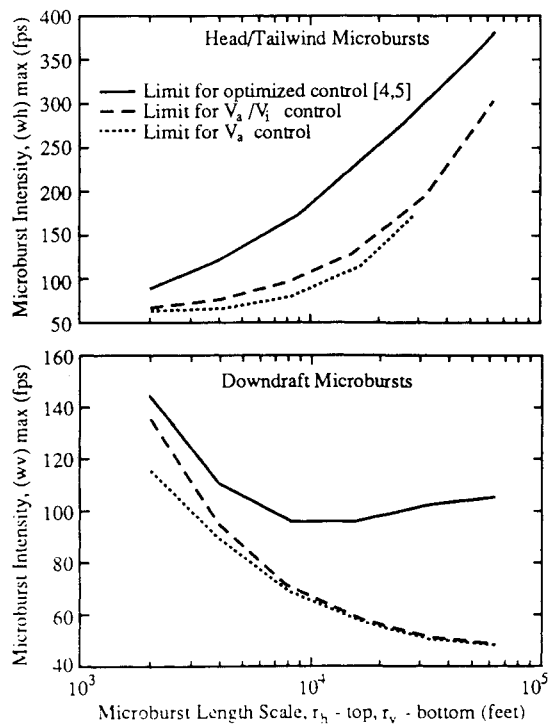

Fig. 7 Three different length-scale vs intensity performance contours in headwind/tailwind and downdraft microbursts.

until sometime into the microburst encounter. In fact, the V_a guidance law sometimes reduces thrust from its nominal setting during significant portions of an encounter. Nevertheless, the performance results for the practical control laws are encouraging. The microburst that downed the Delta Air Lines L1011 at Dallas/Ft. Worth in 1985[2] probably could have been negotiated successfully with the V_a/V_i thrust guidance law and the aircraft of this paper ($r_h \sim 17{,}000$ ft, $w_{h_{max}} \sim 60$ fps, $r_v \sim 8000$ ft, $w_{v_{max}} \sim 35$ fps).

Another similarity between the plots of Fig. 7 is that the V_a/V_i thrust guidance law always yields performance contours higher in microburst intensity than those of the V_a law. The V_a/V_i contours are as much as 20% higher than the V_a contours for headwind/tailwind microbursts of about 10,000 ft length scale. This disparity decreases as length scale increases or decreases from 10,000 ft, but it is very significant, especially since some hazardous microbursts have been measured in this length-scale regime.[17] The V_a/V_i guidance law is superior to the V_a guidance law in the downdraft case as well, but less significantly so.

The superiority of the airspeed/inertial-speed guidance law over the airspeed guidance law exists because the former guidance law calls for more thrust very early in a microburst encounter and maintains higher or equal inertial velocity throughout the encounter. This added inertial velocity helps in headwind/tailwind microbursts by keeping the airspeed above the 1-g stall limit in severe tailwinds. It helps in downdraft microbursts, especially those of shorter length scale, by acting as a reserve of kinetic energy that can be traded for air-relative potential energy in the worst section of the downdraft. The V_a guidance law does call for more thrust than the V_a/V_i guidance law for the second quarter of a headwind/tailwind microburst (the portion of the microburst during which the headwind still exists but is decreasing, Fig. 4). Despite this thrust difference, the inertial speed it loses during the headwind buildup section may not be regained in the headwind dissipation section if the microburst intensity is too high. This is due to thrust saturation.

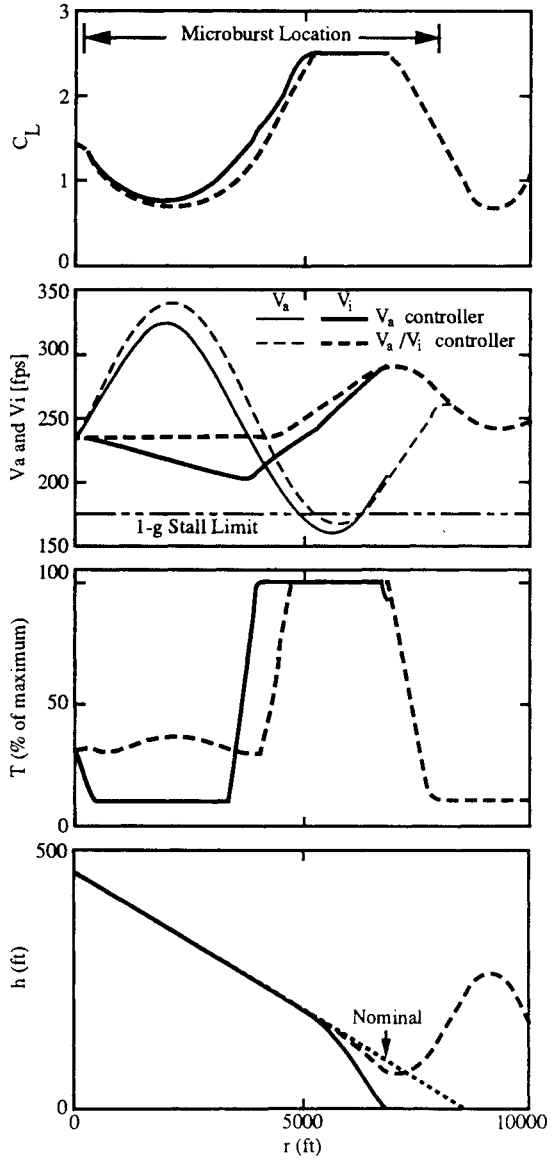

Fig. 8 Sixth-order aircraft model and two thrust control laws in a headwind/tailwind microburst (r_h = 8000 ft, $w_{h_{max}}$ = 105 fps).

Sixth-Order-System Microburst Encounter Examples

This section considers the results for some typical trajectories of the sixth-order aircraft model in conjunction with the controller of Fig. 3. It validates the applicability of the conclusions drawn from the first-order model and further illustrates the performance of the two types of thrust controllers.

Figure 8 presents some time histories for two encounters with the same microburst. The microburst is a very intense headwind/tailwind microburst ($w_{h_{max}}$ = 105 fps, r_h = 8000 ft); it is above the performance range for both controllers—26 fps too intense for the V_a controller, 9 fps too intense for the V_a/V_i controller. The two trajectories correspond to the two different thrust guidance laws (solid for the V_a law, dashed for the V_a/V_i law). The plots are, from the top, lift coefficient, airspeed and inertial speed, thrust, and altitude, all plotted vs range. Note that there is one difference between this model and the first-order model that affects performance: the minimum thrust limit for this model is 10% rather than 0%. This difference makes the sixth-order model more realistic; the engine idle thrust is greater than 0%. Also it will help the performance of the V_a controller by making it less able to slow down in the headwind.

Both controllers encounter difficulties in this microburst. The V_a/V_i-controlled aircraft experiences a 20-ft deviation below the intended glide slope; then it recovers and balloons above the glide slope (bottom plot). At this point a go-around would probably be initiated. The aircraft would be in a favorable position for this. The V_a-controlled aircraft, on the other hand, touches down (crashes?) 1700 ft short of the runway.

The V_a-controller fails to track glide slope because it runs out of airspeed. The V_a/V_i controller fails only because it cannot lower angle of attack quickly enough as the tailwind dissipates at the trailing edge of the microburst. This is caused by the angle-of-attack rate limiting in the sixth-order model's pitch dynamics. The failure to maintain glide slope due to ballooning is probably a more benign failure mode than the short landing failure. Therefore, the airspeed/inertial-speed controller is preferable to the airspeed controller.

This example illustrates the significance of an effect not found in the first-order aircraft model. Angle-of-attack rate limiting seems to play a role mostly during the latter portions of a microburst encounter when the aircraft is recovering from large altitude deviations or when its airspeed is increasing rapidly. Thrust response dynamics and rate limiting do not have a significant effect in the examples that have been considered.

Figure 9 presents some time histories for two encounters with a microburst like that of Miele et al.[9] The microburst, a combination of horizontal and vertical winds, corresponds to $w_{h_{max}}$ = 80 fps, r_h = 8000 ft, $w_{v_{max}}$ = 80 fps, r_v = 4000 ft. It has some deviations from the form shown in Fig. 2 that make it more like Miele's microbursts. It has no headwind buildup section at the beginning of the microburst nor any tailwind dissipation section at the end. The headwind is uniform at 80 fps before entering the microburst, and the tailwind is uniform at 80 fps after exit from the microburst. The headwind dissipation section and the tailwind buildup section, the two middle quarters, are like those of Fig. 2. The downdraft range depen-

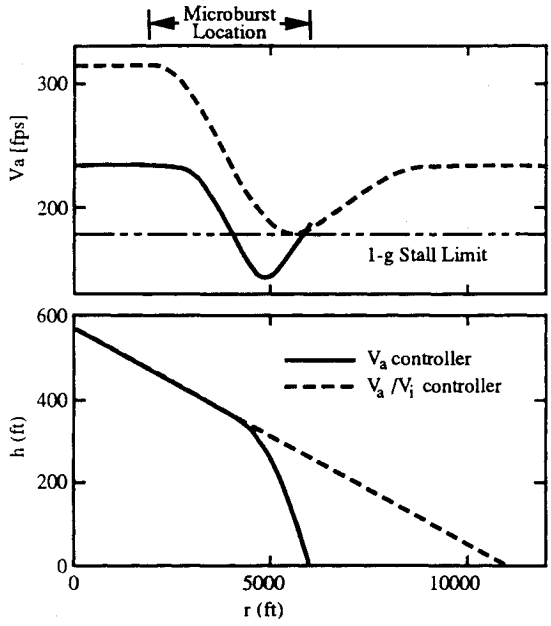

Fig. 9 Sixth-order aircraft model and two thrust control laws in a Miele-type microburst ($\lambda = 1.6$, $w_{h_{max}} = 80$ fps).

dence is like that of Fig. 2, but the downdraft intensity is proportional to altitude. The full 80-fps downdraft applies at $h = 1000$ ft, but the downdraft dwindles to zero at ground level. This microburst is roughly equivalent to a Miele microburst with Miele's intensity parameter λ set equal to 1.6 (a high value).

The two sets of trajectories again correspond to the two different thrust guidance laws (solid for the V_a law, dashed for the V_a/V_i law). The top plot is airspeed, and the bottom plot is altitude, both plotted vs range. Note that the initial conditions of the two cases are different. In the V_a case, the airspeed is initially 235 fps and the inertial speed is about 155 fps. In the V_a/V_i case, the inertial speed is initially 235 fps and the airspeed is about 315 fps. These initial conditions immediately give a large advantage to the V_a/V_i controller, but they are the only initial conditions consistent with the actions that the respective controllers would have taken before encountering the microburst.

The airspeed/inertial-speed controller again performs far better than the airspeed controller, mostly by virtue of having more inertial speed when entering the microburst. The V_a/V_i-controlled aircraft experiences insignificant deviation from the intended glide slope and touches down on the runway (bottom plot). The V_a-controlled aircraft crashes a mile short of the runway. The V_a/V_i-controlled aircraft has a fairly high inertial speed when it touches down: 315 fps. If this is too fast, it is in a good position to execute a go-around.

Conclusions

Two practical guidance laws for microburst wind shear encounter on the landing approach have been presented and analyzed in this paper. Each controls glide slope with pitch inputs, tightly regulating altitude to follow the nominal glide slope. One, called the airspeed law, uses thrust to keep airspeed at a nominal value. The other, called the airspeed/inertial-speed law, uses thrust to keep the minimum of (airspeed, inertial speed) at a nominal value. The airspeed/inertial-speed guidance law performs better than the airspeed guidance law in severe microbursts that cause thrust saturation, especially in severe headwind/tailwind microbursts. This is because the former controller allows the airspeed to rise in the headwind buildup section of a microburst, whereas the latter controller is "fooled" into decreasing thrust in this same section of a microburst. Both controllers perform identically in the absence of winds because airspeed equals inertial speed in this case. A performance analysis of the two controllers bears out the conclusion that the airspeed/inertial-speed guidance law is better than the airspeed guidance law for two classes of microbursts. The airspeed/inertial-speed guidance law, coupled with the flight-path controlling pitch law, is a good, practical microburst encounter strategy.

This conclusion about the use of inertial speed in addition to airspeed implies that standard landing approach practices should be changed. A headwind at an airport should be used to provide an increased airspeed margin on landing approach rather than a decreased ground speed at touchdown. The routine inertial speeds envisioned would not exceed the typical values for a no-winds touchdown unless the aircraft actually encountered a microburst. A greater microburst survivability is worth the expense of extra braking distance during routine touchdowns.

References

[1]Fujita, T. T., and Carcena, F., "Analysis of Three Weather-Related Aircraft Accidents," *Bulletin of the American Meteorological Society*, Vol. 58, No. 11, 1977, pp. 1164–1181.

[2]Bach, R. E., Jr., and Wingrove, R. C., "The Analysis of Airline Flight Records for Winds and Performance with Application to the Delta 191 Accident," *AIAA 13th Atmospheric Flight Mechanics Conference*, AIAA, New York, 1986; also, AIAA Paper 86-2227, Aug. 1986.

[3]"Pan American World Airways, Inc., Clipper 759, Boeing 727-235, N4737, New Orleans International Airport, Kenner Louisiana, July 9, 1982," National Transportation Safety Board, Aircraft Accident Rept. 83/02, Washington, DC, March 1983.

[4]Psiaki, M. L., and Stengel, R. F., "Optimal Aircraft Performance During Microburst Encounter," *Journal of Guidance, Control, and Dynamics*, Vol. 14, No. 2, 1991, pp. 440–446.

[5]Psiaki, M. L., "Control of Flight Through Microburst Wind Shear Using Deterministic Trajectory Optimization," Ph.D. Thesis, Princeton Univ., Princeton, NJ, 1987.

[6]Miele, A., Wang, T., and Melvin, W. W., "Guidance Strategies for Near-Optimum Take-Off Performance in a Windshear," *Journal of Optimization Theory and Applications*, Vol. 50, No. 1, 1986, pp. 1–47.

[7]Miele, A., Wang, T., and Melvin, W. W., "Optimal Take-Off Trajectories in the Presence of Windshear," *Journal of Optimization Theory and Applications*, Vol. 49, No. 1, 1986, pp. 1–45.

[8]Miele, A., Wang, T., and Melvin, W. W., "Optimization and Acceleration Guidance of Flight Trajectories in a Windshear," *Journal of Guidance, Control, and Dynamics*, Vol. 10, No. 4, 1987, pp. 368–377.

[9]Miele, A., Wang, T., and Melvin, W. W., "Penetration Landing Guidance Trajectories in the Presence of Windhshear," *Journal of Guidance, Control, and Dynamics*, Vol. 12, No. 6, 1989, pp. 806–814.

[10]Miele, A., Wang, T., Melvin, W. W., and Bowles, R. L., "Acceleration, Gamma, and Theta Guidance for Abort Landing in a Windshear," *Journal of Guidance, Control, and Dynamics*, Vol. 12, No. 6, 1989, pp. 815–821.

[11] Zhao, Y., and Bryson, A. E., "Optimal Paths Through Downbursts," *Journal of Guidance, Control, and Dynamics*, Vol. 13, No. 5, 1990, pp. 813–818.

[12]Zhao, Y., and Bryson, A. E., "Control of an Aircraft in Downbursts," *Journal of Guidance, Control, and Dynamics*, Vol. 13, No. 5, 1990, pp. 819–823.

[13]Psiaki, M. L., and Stengel, R. F., "Analysis of Aircraft Control Strategies for Microburst Encounter," *Journal of Guidance, Control, and Dynamics*, Vol. 8, No. 5, 1985, pp. 553–559.

[14]Psiaki, M. L., and Stengel, R. F., "Optimal Flight Paths Through Microburst Wind Profiles," *Journal of Aircraft*, Vol. 23, No. 8, 1986, pp. 629–635.

[15]McCormick, B. W., *Aerodynamics, Aeronautics, and Flight Mechanics*, Wiley, New York, 1979.

[16]Etkin, B., *Dynamics of Flight*, Wiley, New York, 1982.

[17]Frost, W., Chang, H. P., Elmore, K. L., and McCarthy, J., "Microburst Wind Shear Models from Joint Airport Weather Studies (JAWS)," Federal Aviation Administration, Washington, DC, PM-85-18, June 1985.

[18]Lambregts, A. A., "Functional Integration of Vertical Flight Path and Speed Control Using Energy Principles," NASA CP-2296, March 1984, pp. 389–409.

[19]Shinar, J., private communication, May 1990.